Hysteretic temperature sensitivity of wetland CH_4 fluxes explained by substrate availability and microbial activity

Kuang-Yu Chang*,
Climate and Ecosystem Sciences Division, Lawrence Berkeley National Laboratory, Berkeley, California, USA

William J. Riley,
Climate and Ecosystem Sciences Division, Lawrence Berkeley National Laboratory, Berkeley, California, USA

Patrick M. Crill,
Department of Geological Sciences and Bolin Centre for Climate Research, Stockholm University, Stockholm, Sweden

Robert F. Grant,
Department of Renewable Resources, University of Alberta, Edmonton, Alberta, Canada

Scott R. Saleska
Department of Ecology and Evolutionary Biology, University of Arizona, Tucson, Arizona, USA

*Corresponding author: Kuang-Yu Chang, ckychang@lbl.gov
Climate and Ecosystem Sciences Division, Lawrence Berkeley National Laboratory
Berkeley, California, USA
Phone: (510) 495-8141

Key words: Methane cycling; microbial dynamics; climate change; IsoGenie Project; Stordalen Mire

Abstract

Methane (CH_4) emissions from wetlands are likely increasing and important in global climate change assessments. However, contemporary terrestrial biogeochemical model predictions of CH_4 emissions are very uncertain, at least in part due to prescribed temperature sensitivity of CH_4 production and emission. While statistically consistent apparent CH_4 emission temperature dependencies have been inferred from meta-analyses across microbial to ecosystem scales, year-round ecosystem-scale observations have contradicted that finding. Here, we show that apparent CH_4 emission temperature dependencies inferred from year-round chamber measurements exhibit substantial intra-seasonal variability, suggesting that using static temperature relations to predict CH_4 emissions is mechanistically flawed. Our model results indicate that such intra-seasonal variability is driven by substrate-mediated microbial and abiotic interactions: seasonal cycles in substrate availability favors CH_4 production later in the season, leading to hysteretic temperature sensitivity of CH_4 production and emission. Our findings demonstrate the uncertainty of inferring CH_4 emission or production rates from temperature alone, and highlight the need to represent microbial and abiotic interactions in wetland biogeochemical models.

1. Introduction

Methane (CH_4) is the second most important climate forcing gas with at least a 28-fold higher global warming potential (GWP) than carbon dioxide (CO_2) over a 100-year horizon (Myhre, *et al* 2013). Atmospheric CH_4 concentrations have more than doubled since 1750 (Saunois et al., 2016) and have contributed about 20% of the additional radiative forcing accumulated in the lower atmosphere (Ciais et al., 2013). Recent assessments have found that CH_4 emissions from wetland and other inland waters are the largest and most uncertain sources affecting the global CH_4 budget (Kirschke et al., 2013; Poulter et al., 2017; Saunois et al., 2016). Such CH_4 emissions account for 25 to 32% of current global total CH_4 emissions (Saunois et al., 2016) and contribute substantially to the renewed and sustained atmospheric CH_4 growth after 2006 (Saunois et al., 2017). Increasing CH_4 emissions could offset mitigation efforts and accelerate climate change (Bastviken et al., 2011; Kirschke et al., 2013) due to their strong influence on the global radiative energy budget (Neubauer and Megonigal, 2015). However, CH_4 emission estimates are poorly constrained due to insufficient quality-controlled measurements (Bastviken et al., 2011; Kirschke et al., 2013; Saunois et al., 2016) and uncertain model structures and parameterizations (Melton et al., 2013; Wania et al., 2013; Xu et al., 2016). In fact, simulations in the ongoing Coupled Model Intercomparison Project Phase 6 (CMIP6; (Eyring et al., 2016)) do not even request wetland CH_4 emission predictions for the historical or 21st century periods. A number of knowledge gaps (Xu et al., 2016) need to be addressed to improve CH_4 model representations and thereby CH_4 climate feedback predictions (Dean et al., 2018). Such efforts are imperative because, among other reasons, permafrost degradation resulting from observed global-scale

64 permafrost warming (Biskaborn et al., 2019) can stimulate organic matter decomposition
65 (Schuur et al., 2015) that could augment global warming with a strong contribution from
66 CH_4 (Knoblauch et al., 2018).

67 Many contemporary terrestrial biogeochemical models parameterize CH_4
68 production (or even CH_4 emissions) as a static temperature function of net primary
69 production or heterotrophic respiration (Melton et al., 2013; Wania et al., 2013; Xu et al.,
70 2016). Such parameterization is supported by recent meta-analyses that indicate a static
71 and consistent apparent CH_4 production and emission temperature dependence across
72 microbial to ecosystem scales (Yvon-Durocher et al., 2014). However, measurements
73 collected across sites with nearly identical wetland climate, hydrology, and plant
74 community compositions suggest large spatial and temporal variability in the ratio
75 between ecosystem productivity and CH_4 emissions (Hemes et al., 2018). Further,
76 ecosystem-scale CH_4 emissions have hysteretic responses to seasonal changes in gross
77 primary productivity (GPP), water table depth (WTD), and temperature (Brown et al.,
78 2014; Goodrich et al., 2015; Rinne et al., 2018; Zona et al., 2016), suggesting that CH_4
79 biogeochemistry may not be accurately represented by static relationships. Consequently,
80 a mechanistic understanding of factors modulating CH_4 production and emission rates is
81 urgently needed to improve the currently uncertain CH_4 biogeochemistry
82 parameterization.

83 Although observations of changes in CH_4 production, oxidation, and emission
84 rates; spatial heterogeneity; and seasonal dynamics following permafrost degradation
85 have been discussed (Hodgkins et al., 2014; McCalley et al., 2014; Olefeldt et al., 2013;
86 Perryman et al., 2020), an understanding of mechanisms regulating intra-seasonally

varying CH_4 emissions and their response to temperature is still lacking. We therefore investigated the impacts of soil thermal and hydrological history on CH_4 emissions to improve understanding of apparent CH_4 emission temperature dependence and inform CH_4 model structure and parameterization. We hypothesized that a static apparent CH_4 emission temperature dependence is not sufficient for modeling CH_4 emissions due to substrate-mediated hysteretic microbial and abiotic interactions (Tang and Riley, 2014) over seasonal time scales. We used a comprehensive biogeochemistry model (*ecosys*) to investigate observed intra-seasonal changes in apparent CH_4 emission temperature dependence at two high-latitude sites: Stordalen Mire (68.2 °N, 19.0 °E) and Utqiaġvik (formerly Barrow, 71.3 °N, 156.5 °W). We focus most of the detailed analysis at Stordalen Mire, where we recently validated the modeled CH_4 production pathways using acetoclastic and hydrogenotrophic methanogen relative abundance inferred from 16S rRNA gene amplicon sequencing data (Chang et al., 2019b). We also evaluated the uncertainty of ignoring substrate-mediated hysteretic microbial and abiotic interactions.

2. Methods

2.1 Study site description

The Stordalen Mire sites are about 10 km east of the Abisko Scientific Research Station in the discontinuous permafrost zone of northern Sweden and include intact permafrost palsa, partly thawed bog, and fen (Hodgkins et al., 2014). The mean annual air temperature and precipitation at the Stordalen Mire are around 0.6 °C and 336 mm y^{-1}, respectively. The measured CH_4 emissions are near zero in the palsa due to its deeper WTD and shallower Active Layer Depth (ALD) (Bäckstrand et al., 2008b, 2008a, 2010); we therefore did not include this site in our analysis. The bog is ombrotrophic (pH ~4.2)

110 with WTD fluctuating from the peat surface to 35 cm below the peat surface (Bäckstrand
111 et al., 2008b, 2008a; Olefeldt and Roulet, 2012), and is dominated by *Sphagnum* spp.
112 mosses with a moderate abundance of short sedges such as *Eriophorum vaginatum* and
113 *Carex bigelowii* (Bäckstrand et al., 2008b, 2008a; Malmer et al., 2005; Olefeldt and
114 Roulet, 2012). The fen is minerotrophic (pH~5.7), has WTD near or above the peat
115 surface throughout the growing season, and is dominated by tall sedges such as *E.*
116 *angustifolium*, *C. rostrata* and *Esquisetum* spp. (Bäckstrand et al., 2008b, 2008a; Olefeldt
117 and Roulet, 2012). The Stordalen Mire bog and fen both have a peat layer ranging from
118 0.5 to 1 m (Rydén and Kostov, 1980) and an ALD greater than 0.9 m (Bäckstrand et al.,
119 2008b).

120 The Utqiaġvik site is located at the Barrow Experimental Observatory at the
121 northern tip of Alaska's Arctic coastal plain, which is characterized by polygonal
122 landforms caused by seasonal freezing and thawing of tundra soil (Hinkel et al., 2005).
123 These polygonal landforms were categorized into separate features based on moisture
124 variation determined by surface elevations (Wainwright et al., 2015). We analyzed CH_4
125 emissions modeled in the low-centered polygonal landform that was represented as a
126 connected combination of trough, rim, and center structures (Grant et al., 2017b). The
127 mean annual air temperature and precipitation at Utqiaġvik are around -12°C and 106
128 mm y^{-1}, respectively. The ALD varies spatially from approximately 20 to 60 cm, which is
129 influenced by soil texture, vegetation, soil moisture, and inter-annual variability
130 (Shiklomanov et al., 2010).

131 **2.2 Field measurements**

A system of six automated gas-sampling chambers made of transparent Lexan was installed at the Stordalen Mire in 2001 (three in the bog and three in the fen). Each chamber covered an area of 0.14 m^2 (38 cm× 38 cm) with a height of 25–45 cm depending on the vegetation and the depth of insertion, and was closed for 5 minutes every 3 hours. In addition, each chamber is instrumented with thermocouples measuring air and ground surface temperatures, and WTD is measured manually three to five times per week from June to October each year (McCalley et al., 2014). The system was updated with a new chamber design similar to that described in (Bubier et al., 2003) in 2011. The new chambers each cover an area of 0.2 m^2 (45 cm× 45 cm), with a height ranging from 15 to 75 cm depending on habitat vegetation.

2.3 Apparent temperature dependence calculation

We quantify the apparent temperature dependencies of daily CH_4 emission and CH_4 production by fitting Boltzmann-Arrhenius functions of the form:

$$\ln F_i(T) = \overline{E_{a,i}} \cdot \left(\frac{-1}{kT}\right) + \varepsilon_{F_i} \quad \text{(Eq. 1)}$$

where $F_i(T)$ is the rate of CH_4 emission (i = 1) and CH_4 production (i = 2) at absolute temperature T. $\overline{E_{a,i}}$ (in eV) and ε_{F_i} correspond to the fitted apparent activation energy (slope) and base reaction rate (intercept), respectively. k is the Boltzmann constant (8.62× 10^{-5} eV K^{-1}).

We defined earlier and later periods as the times before and after the highest daily temperature analyzed in a given thawed season, respectively, to quantify intra-seasonal changes in apparent CH_4 emission or production temperature dependencies. Thawed seasons were defined as the time period when measured or modeled temperatures are at least 1 °C to avoid low CH_4 emissions in the 0 – 1 °C temperature window that can alter

155 the base reaction rate of our Boltzmann-Arrhenius functions. Four types of temperature
156 were used in our analysis: (1) measured soil surface temperature (e.g., Fig. 1), (2)
157 modeled vertical mean 0 – 20 cm soil temperature (e.g., Fig. 2), (3) measured air
158 temperature (e.g., Supplementary Fig. 1), and (4) modeled air temperature (e.g.,
159 Supplementary Fig. 2). The vertical mean 0 – 20 cm soil temperature was chosen for our
160 analysis because CH_4 production at our study site is concentrated in the top 20 cm of soil
161 (Chang et al., 2019b). Consistent hysteretic temperature responses were derived with
162 above zero vertical mean 0 – 20 cm soil temperatures (i.e., include the modeled 0 – 1 °C
163 temperature window), e.g., Fig. 2 vs. Supplementary Fig. 3.

164 **2.4 Model description**

165 The *ecosys* model is a comprehensive biogeochemistry model that explicitly
166 represents interactions among biogeophysical (i.e., hydrological and thermal),
167 biogeochemical (including carbon, nitrogen, and phosphorus), plant and microbial
168 processes. The above-ground processes are represented in multi-specific multi-layer plant
169 canopies, and the below-ground processes are represented in multiple soil layers with
170 multiphase subsurface reactive transport. CH_4 production (i.e., acetoclastic and
171 hydrogenotrophic methanogenesis), CH_4 oxidation, and CH_4 transport (i.e., diffusion,
172 aerenchyma, and ebullition) are explicitly represented in *ecosys*. The *ecosys* model
173 operates at variable time steps (~seconds to 1 hour) determined by convergence criteria,
174 and it can be applied at patch scale (spatially homogenous one-dimensional; e.g., (Chang
175 et al., 2019a)) and landscape scale (spatially variable two- or three-dimensional; e.g.,
176 (Grant et al., 2017b, 2017a)). The *ecosys* model has been extensively examined against
177 field measurements made in 2002–2007 (Chang et al., 2019a) and 2011–2013 (Chang et

178 al., 2019b) at our study sites at the Stordalen Mire, and 2013 at our study sites at
179 Utqiagvik (Grant et al., 2017b, 2017a, 2019). A qualitative summary of the *ecosys* model
180 is provided in the supplementary material to this article, and detailed descriptions are
181 available in the supplements of (Grant et al., 2017b, 2017a). The *ecosys* model structure
182 remains unchanged from that in earlier studies.

183 **2.5 Experimental design**

184 The primary purpose of this study is to explore the implications of the observed
185 CH_4 emission hysteresis (Fig. 1) and highlight the need to recognize factors other than
186 temperature that control ecosystem-scale CH_4 emissions. We develop a mechanistic
187 explanation for such hysteresis by investigating how the modeled environmental drivers
188 modulate CH_4 emission hysteresis. The modeled data used in this study are extracted
189 from our earlier simulations that can be downloaded from the IsoGenie database
190 (https://isogenie-db.asc.ohio-state.edu/; (Chang et al., 2019a, 2019b)) and the NGEE-
191 Arctic database (https://ngee-arctic.ornl.gov/; (Chang and Riley, 2020; Grant et al.,
192 2017b, 2017a). Our analysis focuses on modeled data because some factors (e.g., root
193 exudates, substrate availability, and methanogenic population and activity) modulating
194 CH_4 production, oxidation, and emission rates are not continuously measured at our study
195 sites. Our recently published model results at the Stordalen Mire and Utqiaġvik sites
196 indicate good comparisons with observations, including for thaw depth (R^2 = 0.75 to
197 0.90), WTD (mean bias = -4.3 to 4.0 cm), and CO_2 (R^2 = 0.43 to 0.88) and CH_4 (R^2 =
198 0.31 to 0.93) surface fluxes (Chang et al., 2019a, 2019b; Grant et al., 2017b, 2017a,
199 2019). In particular, CH_4 production pathway modeled at our Stordalen Mire sites has
200 been validated by the relative abundances of acetoclastic and hydrogenotrophic

methanogenic lineages reported in McCalley et al. (2014), suggesting that substrate and microbial dynamics are reasonably represented. For conciseness, we focus discussion in the remainder of the paper on the Stordalen Mire fen site, since it exhibits strong apparent hysteresis and the underlying mechanisms leading to hysteretic CH_4 emissions are similar across all study sites.

We note the relevant point that the *ecosys* model itself represents temperature dependence of soil metabolic activity and gas production through locally simulated soil temperature profiles with an modified Arrhenius function that includes terms for low- and high-temperature inactivation (Grant, 2015). Besides temperature effects, the *ecosys* model also represents substrate controls (through Michaelis-Menten kinetics) on microbial biomass and activity (e.g., Chang et al., 2019b), which is not explicitly characterized by inferring an apparent whole system temperature dependence (e.g., Eq. 1). These representations allow the model to simulate overall CH_4 emission patterns with more complex dynamics than represented in the apparent temperature dependence function alone, making it a suitable tool for investigating the relative importance of temperature dependence versus other factors.

3. Results and discussion

3.1 Observed patterns of apparent CH_4 emission hysteresis

The CH_4 emissions measured in the Stordalen Mire bog and fen exhibit hysteretic responses to soil surface temperature: i.e., at the same soil surface temperature, greater CH_4 emissions during the later than the earlier periods of the thawed season (Fig. 1). At both sites, plotting time- and chamber- specific CH_4 emission and soil surface temperature measurements from the beginning to end of the thawed season results in a

counterclockwise hysteresis loop at each site-year (2012 to 2017). Such hysteretic responses lead to intra-seasonally varying apparent CH_4 emission temperature dependencies, suggesting that a proper representation of temporal variability is needed to recognize factors modulating CH_4 emissions. For example, three distinct apparent CH_4 emission temperature dependencies can be derived from the same chamber sampling at different periods within the same thawed season (i.e., earlier period, later period, and full season). Despite the high spatial heterogeneity, the observed patterns of CH_4 emission hysteresis are consistent across chambers within and between the bog and fen habitats. Our results thus demonstrate that CH_4 emissions are generally more sensitive to temperature changes during the later part of the thawed season, and that CH_4 emission strength and temperature dependence vary substantially among site-years. Consistent hysteretic responses can be found in CH_4 emission and air temperature measurements (Supplementary Fig. 1), suggesting that the apparent CH_4 emission hysteresis is not dependent on time lags between air and soil temperatures (Wohlfahrt and Galvagno, 2017). The observed CH_4 emission hysteresis indicates that models cannot accurately represent CH_4 dynamics without representing the large spatial and temporal variability in apparent CH_4 emission temperature dependencies.

3.2 Modeled patterns of apparent CH_4 emission hysteresis

The CH_4 emissions modeled by *ecosys*, extracted from our recently published results at the Stordalen Mire and the Utqiaġvik sites (Chang et al., 2019b; Grant et al., 2017b), have hysteretic responses to mean 0–20 cm soil temperature (Fig. 2) and air temperature (Supplementary Fig. 2). The apparent CH_4 emission temperature dependence inferred from the modeled results varies substantially from the beginning to the end of the

thawed season, suggesting that CH_4 emissions may not be accurately represented as a single function of temperature. For each site-year, CH_4 emissions modeled in the later period are greater than those in the earlier period at the same temperature (e.g., Fig. 2), consistent with observations (e.g., Fig. 1). The apparent CH_4 emission hysteresis is larger and clearer in the Stordalen Mire fen compared to the bog and the Utqiaġvik low-centered polygon, likely from its warmer soil temperatures, shallower WTD, and higher CH_4 emissions (Chang et al., 2019b). Consistent hysteresis patterns are found at weekly timescales (Supplementary Fig. 4), suggesting that the apparent CH_4 emission hysteresis is not sensitive to temporal resolution nor the timing of maximum seasonal temperature. In addition to temporal variability, changes in biogeophysical conditions driven by fine-scale hydrology and vegetation differences can also alter the apparent functional relationship between CH_4 emission and temperature. For example, apparent CH_4 emission temperature dependencies inferred for individual topographic features (i.e., troughs, rims, and centers) vary substantially within the same wetland ecosystem at Utqiaġvik (Supplementary Fig. 5).

We evaluate the effects of intra-seasonal variability on ecosystem-scale CH_4 emissions by estimating apparent CH_4 emission temperature dependencies during different parts of the thawed season. By fitting the Boltzmann-Arrhenius function (Eq. 1) to the CH_4 emissions and 0–20 cm soil temperatures modeled during different time frames (i.e., earlier period, later period, and full season), we developed and evaluated three temperature dependence models for each thawed season. Our results show that CH_4 emission estimates improve when apparent CH_4 emission temperature dependencies were separately represented in the earlier and later periods, compared to those assuming a

seasonally invariant apparent CH_4 emission temperature dependence (Supplementary Table 1, 2). In the Stordalen Mire, neglecting intra-seasonal variability in apparent CH_4 emission temperature dependence leads to overestimated (10 to 81%) and underestimated (-21 to -40%) CH_4 emissions during the earlier and later periods, respectively (Supplementary Table 1). Consistent prediction bias was found in the Utqiaġvik low-centered polygon, except in the rims where drier conditions limit CH_4 emissions (Supplementary Table 2).

These results demonstrate that models based on a seasonally invariant apparent CH_4 emission temperature dependence may introduce errors by improperly prescribing the seasonal dynamics of CH_4 biogeochemistry with a static function of temperature. The substantial intra-seasonal variability, potentially led by site specific thermal and hydrological history (Updegraff et al., 1998), could be an important and overlooked property of natural wetlands that currently account for 25 to 32% of global total CH_4 emissions (Saunois et al., 2016). Representing intra-seasonally variable apparent CH_4 emission or production temperature dependencies in large-scale wetland biogeochemical models may thus reduce CH_4 emission prediction biases and model structural uncertainty.

3.3 Microbial substrate-mediated CH_4 production hysteresis

For conciseness, we focus our discussion on the potential drivers causing the hysteretic relationship between CH_4 emission and soil temperature modeled at the Stordalen Mire fen at 2011, as the underlying mechanisms are consistent across all site-years. The temporal evolution of CH_4 emissions modeled by *ecosys* follows that of CH_4 production, with limited offsets from CH_4 oxidation (Fig. 3a). Modeled CH_4 emission (e.g., Fig. 2d) and production (Fig. 3b) rates both exhibit intra-seasonal variations in their

293 apparent temperature dependencies during the thawed season, consistent with the varying
294 temperature responses to microbial thermal history reported in laboratory incubations
295 (Updegraff et al., 1998). The relatively low CH_4 oxidation suggests that hysteretic
296 responses of modeled CH_4 emissions to temperature (Fig. 2) primarily result from
297 hysteretic CH_4 production (Fig. 3b) associated with asymmetric methanogen biomass
298 (Fig. 3c) and activity (Fig. 3d) between the earlier and later periods. Further, the
299 consistent seasonal cycles in CH_4 production, oxidation, and emission rates modeled
300 from 2011 to 2013 (Supplementary Fig. 6) indicate that the CH_4 emission hysteresis
301 modeled in that period (Fig. 2d, e, f) is not caused by relatively low CH_4 oxidation
302 modeled in a particular site-year. This result is consistent with isotopic measurements
303 which also indicated that changes in CH_4 production, not CH_4 oxidation, determine the
304 CH_4 emissions observed in the Stordalen Mire sites (McCalley et al., 2014).

305 Although CH_4 oxidation has been proposed to be an important control regulating
306 wetland CH_4 emissions, e.g., Perryman et al. (2020) and Singleton et al. (2018), the
307 competitive dynamics between methanogens and methanotrophs throughout the year has
308 not been included in such studies. The modeled CH_4 oxidation rate is relatively low
309 during the thawed season when CH_4 production is strongest, and relatively high during
310 the shoulder season when CH_4 production is weakest (Supplementary Fig. 6). These
311 strong seasonal variations suggest that the relative importance of CH_4 production and
312 oxidation on regulating CH_4 emissions may fluctuate throughout the year, highlighting
313 the need to properly represent the underlying dynamics controlling CH_4 biogeochemistry.

314 Increased soil temperatures elevate oxygen demands for aerobic heterotrophs
315 while reducing oxygen solubility, which favors fermenter and methanogens and thereby

316 enhance CH_4 production. Our model results indicate that the elevated methanogen
317 biomass and activity during the later period are driven by the increased substrate
318 availability for methanogenesis later in the thawed season. Specifically, modeled
319 substrate concentrations remain relatively high after peak substrate production rate at
320 maximum seasonal soil temperature for both acetoclastic (AM; Fig. 4a) and
321 hydrogenotrophic methanogenesis (HM; Fig. 5a). Relatively high AM (Fig. 4b) and HM
322 (Fig. 5b) substrate availability during the later period elevates AM and HM energy yields
323 at a given soil temperature, resulting in higher methanogen growth (Fig. 3d) and biomass
324 (Fig. 3c) later in the thawed season. Therefore, CH_4 production rates during the later
325 period become higher than those during the earlier period at the same soil temperature
326 (Fig. 3b), which drives higher CH_4 emissions with increased aqueous CH_4 concentrations.
327 Although AM and HM each exhibit microbial substrate-mediated hysteretic temperature
328 responses, AM appears to be more hysteretic to soil temperature than HM (Fig. 6). The
329 stronger AM hysteresis is consistent with the larger and clearer CH_4 emission hysteresis
330 found in the Stordalen Mire fen (Fig. 2), where the fractional contribution of AM to total
331 CH_4 production is higher than in the Stordalen Mire bog (Chang et al., 2019b; McCalley
332 et al., 2014). A schematic summarizing the above-mentioned mechanisms for microbial
333 substrate-mediated CH_4 production hysteresis is presented in Fig. 7.
334 Although the CH_4 emission rates and CH_4 production pathways modeled in the
335 Stordalen Mire fen have been examined (Chang et al., 2019b), continuous substrate
336 concentration measurements are lacking for validating the substrate-mediated hysteretic
337 temperature responses proposed here. Wide ranges of acetate and hydrogen
338 concentrations have been reported from incubation experiments studying methanogenesis

(e.g., Hines et al., 2008; Tøsdal et al., 2015; Zhang et al., 2020); however, those values may not be used to validate the time and space specific substrate concentrations modeled at our study sites. Therefore, further studies and additional field measurements are needed to test our proposed hypothesis of the causes of observed CH_4 emission hysteresis.

3.4 Other factors regulating intra-seasonal CH_4 emissions

To evaluate whether microbial substrate-mediated CH_4 production hysteresis is the primary cause of the observed hysteretic relationship between CH_4 emission and temperature, we evaluated four alternative hypotheses: interactions with (1) water table depth; (2) GPP (via exudation, root litter inputs, and aerenchyma development); (3) thaw depth; and (4) residual pore-water CH_4 concentrations at the end of the earlier part of the thawed season.

First, studies have found that seasonal variations of WTD determine CH_4 cycling dynamics by regulating the temperature response of CH_4 emissions, leading to hysteretic CH_4 emissions when drought-induced WTD drawdown below the critical zone for CH_4 production (Brown et al., 2014; Goodrich et al., 2015). The substantial CH_4 emission hysteresis observed in the Stordalen Mire fen is unlikely caused by seasonal variations in WTD, because the observed WTD are around or above the peat surface throughout the thawed season with limited effects on CH_4 emissions (Bäckstrand et al., 2008b).

Second, Rinne et al. (2018) reported that the temporal variations of CH_4 emissions are strongly regulated by GPP, and the time required to convert GPP to methanogenesis substrates may cause the observed apparent hysteresis found between GPP and CH_4 emissions. Such apparent hysteresis was also modeled at our study sites (e.g., Fig. 8a), which shows higher CH_4 emissions later in the thawed season at a given

GPP. We further analyzed factors linking GPP and CH_4 emissions modeled at the Stordalen Mire fen to explore whether an apparent hysteretic relationship between CH_4 emissions and GPP is causally connected. We examined three primary pathways by which GPP could lead to a delayed effect on CH_4 emissions, and thereby apparent hysteresis: increases in (1) fresh carbon inputs from root exudation (Fig. 8b), (2) below-ground litter inputs (Fig. 8c), and (3) aerenchyma transport caused by GPP-induced growth of porous sedge roots (Fig. 8d). In contrast to the apparent hysteresis with GPP, all three of these mechanisms exhibit reversed hysteresis cycles compared to those between CH_4 emissions and temperature. Therefore, these three primary mechanisms are inconsistent with a causal hysteretic relationship between GPP and CH_4 emissions.

Third, studies have suggested that soil temperature increases can expand the volume of unfrozen soil and thereby stimulate deep carbon decomposition, which can also contribute to higher carbon emissions later in the thawed season, as has been observed for upland CO_2 emissions (Goulden et al., 1998) and wetland CH_4 emissions (Iwata et al., 2015). Our results show a weak correlation between thaw depth and CH_4 emissions during the latter part of the thawed season, although CH_4 emissions appear to increase with deeper thaw during the earlier period (Fig. 8e). Therefore, the hysteretic relationship between CH_4 emission and soil temperature found at our study sites is not causally connected with the greater volume of unfrozen soil later in the thawed season. This result may be explained by the relatively shallow zone (mostly within the top 20 cm of soil) of CH_4 production (Chang et al., 2019b) compared with the much deeper thaw depth (> 90 cm) measured and modeled during the peak CH_4 emission period (i.e., July to August) (Chang et al., 2019a).

Fourth, we conducted a sensitivity test to examine the amount of lagged CH_4 emissions resulting from CH_4 residual stored in the soil profile at the end of the earlier part of the thawed season. In the sensitivity test, we turned off CH_4 production during the later part of the thawed season so the later-period CH_4 emissions modeled in this run are driven by lagged releases of earlier-period CH_4 production. At the Stordalen Mire fen, later-period CH_4 emissions resulting from earlier-period CH_4 residual concentrations decreased approximately exponentially and contributed about 25% of the CH_4 emissions during the later period (Fig. 9). The timing and magnitude of later-period CH_4 emissions attributed to lagged CH_4 emissions do not match with the relatively high CH_4 emissions modeled during the later period. Therefore, our results suggest that lagged CH_4 emissions from residual CH_4 produced in the earlier period are not a dominant factor leading to the observed CH_4 emission hysteresis, although lagged CH_4 emissions may amplify the apparent CH_4 emission hysteresis detected in the system.

Collectively, our results suggest that microbial substrate-mediated CH_4 production hysteresis is likely to be the primary control of the observed apparent CH_4 emission hysteresis. The physical controls on CH_4 production and emission (and potentially their hysteresis patterns) in the sediments of terrestrial freshwater systems may differ from those we derived from vegetated peat surfaces (Wik et al., 2016), and further investigation is needed to assess their apparent temperature dependence. To better understand factors controlling CH_4 production and emission, continuous measurements of seasonal development of methanogenesis substrates and soil temperature at the depth where CH_4 production is prevalent are needed.

4. Conclusions

Many contemporary CH_4 models parameterize wetland CH_4 production (or emission) as a fixed fraction of net primary productivity or heterotrophic respiration regulated by a single static function of temperature (Melton et al., 2013; Wania et al., 2013). Our results suggest that such a parameterization is not accurate because it oversimplifies microbial responses to changing thermal and hydrological conditions that modulate wetland CH_4 production and emission rates. More continuous observations across sites are required to assess model prediction uncertainty and the broader extent to which our mechanistic explanations apply. In summary, we found that apparent CH_4 emission temperature dependencies vary from the earlier to later part of the thawed season due to substrate-mediated CH_4 production hysteresis caused by intra-seasonal changes in methanogen biomass and activity. We examined four alternative mechanisms that may contribute to the observed CH_4 emission hysteresis with temperature, and found none of them can exclusively explain the underlying dynamics. Our findings motivate explicit model representations of microbial dynamics that physiologically link microbial and abiotic interactions, as only three of 40 recently reviewed CH_4 models mechanistically represent CH_4 biogeochemistry (Xu et al., 2016).

Acknowledgements

This study was funded by the Genomic Science Program of the United States Department of Energy Office of Biological and Environmental Research under the ISOGENIE (DE-SC0016440) and NGEE-Arctic projects under contract DE-AC02-05CH11231 to Lawrence Berkeley National Laboratory and grants from Swedish VR (Vetenskaprådet) and Swedish FORMAS to PMC. We acknowledge US National Science Foundation MacroSystems program (NSF EF 1241037) support for

autochamber measurements between 2013 and 2017. We thank the Abisko Scientific Research Station of the Swedish Polar Research Secretariat for providing the meteorological data. The data presented in this study are available at the NGEE Arctic Database (doi:10.5440/1635534). The *ecosys* source code is available at Zenodo (doi:10.5281/zenodo.3906642).

References

Bäckstrand, K., Crill, P. M., Mastepanov, M., Christensen, T. R. and Bastviken, D.: Non-methane volatile organic compound flux from a subarctic mire in Northern Sweden, Tellus, Ser. B Chem. Phys. Meteorol., doi:10.1111/j.1600-0889.2007.00331.x, 2008a.

Bäckstrand, K., Crill, P. M., Mastepanov, M., Christensen, T. R. and Bastviken, D.: Total hydrocarbon flux dynamics at a subarctic mire in northern Sweden, J. Geophys. Res. Biogeosciences, doi:10.1029/2008JG000703, 2008b.

Bäckstrand, K., Crill, P. M., Jackowicz-Korczyñski, M., Mastepanov, M., Christensen, T. R. and Bastviken, D.: Annual carbon gas budget for a subarctic peatland, Northern Sweden, Biogeosciences, 7(1), 95–108, doi:10.5194/bg-7-95-2010, 2010.

Bastviken, D., Tranvik, L. J., Downing, J. A., Crill, P. M. and Enrich-Prast, A.: Freshwater methane emissions offset the continental carbon sink, Science (80-.)., 331(6013), 50, doi:10.1126/science.1196808, 2011.

Biskaborn, B. K., Smith, S. L., Noetzli, J., Matthes, H., Vieira, G., Streletskiy, D. A., Schoeneich, P., Romanovsky, V. E., Lewkowicz, A. G., Abramov, A., Allard, M., Boike, J., Cable, W. L., Christiansen, H. H., Delaloye, R., Diekmann, B., Drozdov, D., Etzelmüller, B., Grosse, G., Guglielmin, M., Ingeman-Nielsen, T., Isaksen, K., Ishikawa, M., Johansson, M., Johannsson, H., Joo, A., Kaverin, D., Kholodov, A., Konstantinov, P.,

Kröger, T., Lambiel, C., Lanckman, J. P., Luo, D., Malkova, G., Meiklejohn, I., Moskalenko, N., Oliva, M., Phillips, M., Ramos, M., Sannel, A. B. K., Sergeev, D., Seybold, C., Skryabin, P., Vasiliev, A., Wu, Q., Yoshikawa, K., Zheleznyak, M. and Lantuit, H.: Permafrost is warming at a global scale, Nat. Commun., 10(1), 1–11, doi:10.1038/s41467-018-08240-4, 2019.

Brown, M. G., Humphreys, E. R., Moore, T. R., Roulet, N. T. and Lafleur, P. M.: Evidence for a nonmonotonic relationship between ecosystem-scale peatland methane emissions and water table depth, J. Geophys. Res. Biogeosciences, 119(5), 826–835, doi:10.1002/2013JG002576, 2014.

Bubier, J., Crill, P., Mosedale, A., Frolking, S. and Linder, E.: Peatland responses to varying interannual moisture conditions as measured by automatic CO 2 chambers , Global Biogeochem. Cycles, doi:10.1029/2002gb001946, 2003.

Chang, K.-Y. and Riley, W.: Hysteretic temperature sensitivity of wetland CH4 fluxes explained by substrate availability and microbial activity: Model Archive, Next Gener. Ecosyst. Exp. Arct. Data Collect. Oak Ridge Natl. Lab. U.S. Dep. Energy, Oak Ridge, Tennessee, USA, doi:10.5440/1635534, 2020.

Chang, K.-Y., Riley, W. J., Crill, P. M., Grant, R. F., Rich, V. I. and Saleska, S. R.: Large carbon cycle sensitivities to climate across a permafrost thaw gradient in subarctic Sweden, Cryosph., 13(2), 647–663, doi:10.5194/tc-13-647-2019, 2019a.

Chang, K.-Y., Riley, W. J., Brodie, E. L., McCalley, C. K., Crill, P. M. and Grant, R. F.: Methane Production Pathway Regulated Proximally by Substrate Availability and Distally by Temperature in a High-Latitude Mire Complex, J. Geophys. Res. Biogeosciences, 2019JG005355, doi:10.1029/2019JG005355, 2019b.

Ciais, P., Sabine, C., Bala, G., Bopp, L., Brovkin, V., Canadell, J., Chhabra, A., DeFries, R., Galloway, J., Heimann, M., Jones, C., Quéré, C. Le, Myneni, R. B., Piao, S. and Thornton, P.: Carbon and Other Biogeochemical Cycles, in Climate Change 2013 - The Physical Science Basis, edited by Stocker, T.F., D. Qin, G.-K. Plattner, M. Tignor, S. K. Allen, J. Boschung, A. Nauels, Y. Xia, V. Bex, and P. M. Midgley, pp. 465–570, Cambridge University Press, Cambridge, United Kingdom and New York, NY, USA, Cambridge., 2013.

Dean, J. F., Middelburg, J. J., Röckmann, T., Aerts, R., Blauw, L. G., Egger, M., Jetten, M. S. M., de Jong, A. E. E., Meisel, O. H., Rasigraf, O., Slomp, C. P., in't Zandt, M. H. and Dolman, A. J.: Methane Feedbacks to the Global Climate System in a Warmer World, Rev. Geophys., 56(1), 207–250, doi:10.1002/2017RG000559, 2018.

Eyring, V., Bony, S., Meehl, G. A., Senior, C. A., Stevens, B., Stouffer, R. J. and Taylor, K. E.: Overview of the Coupled Model Intercomparison Project Phase 6 (CMIP6) experimental design and organization, Geosci. Model Dev., 9(5), 1937–1958, doi:10.5194/gmd-9-1937-2016, 2016.

Goodrich, J. P., Campbell, D. I., Roulet, N. T., Clearwater, M. J. and Schipper, L. A.: Overriding control of methane flux temporal variability by water table dynamics in a Southern Hemisphere, raised bog, J. Geophys. Res. Biogeosciences, 120(5), 819–831, doi:10.1002/2014JG002844, 2015.

Goulden, M. L., Wofsy, S. C., Harden, J. W., Trumbore, S. E., Crill, P. M., Gower, S. T., Fries, T., Daube, B. C., Fan, S.-M., Sutton, D. J., Bazzaz, A. and Munger, J. W.: Sensitivity of Boreal Forest Carbon Balance to Soil Thaw, Science (80-.)., 279(5348), 214–217, doi:10.1126/science.279.5348.214, 1998.

Grant, R. F.: Ecosystem CO2 and CH4 exchange in a mixed tundra and a fen within a hydrologically diverse Arctic landscape: 2. Modeled impacts of climate change, J. Geophys. Res. Biogeosciences, 120(7), 1388–1406, doi:10.1002/2014JG002889, 2015.

Grant, R. F., Mekonnen, Z. A., Riley, W. J., Wainwright, H. M., Graham, D. and Torn, M. S.: Mathematical Modelling of Arctic Polygonal Tundra with Ecosys: 1. Microtopography Determines How Active Layer Depths Respond to Changes in Temperature and Precipitation, J. Geophys. Res. Biogeosciences, 122(12), 3161–3173, doi:10.1002/2017JG004035, 2017a.

Grant, R. F., Mekonnen, Z. A., Riley, W. J., Arora, B. and Torn, M. S.: Mathematical Modelling of Arctic Polygonal Tundra with Ecosys: 2. Microtopography Determines How CO2 and CH4 Exchange Responds to Changes in Temperature and Precipitation, J. Geophys. Res. Biogeosciences, 122(12), 3174–3187, doi:10.1002/2017JG004037, 2017b.

Grant, R. F., Mekonnen, Z. A., Riley, W. J., Arora, B. and Torn, M. S.: Modelling climate change impacts on an Arctic polygonal tundra. Part 2: Changes in CO_2 and CH_4 exchange depend on rates of permafrost thaw as affected by changes in vegetation and drainage, J. Geophys. Res. Biogeosciences, 2018JG004645, doi:10.1029/2018JG004645, 2019.

Hemes, K. S., Chamberlain, S. D., Eichelmann, E., Knox, S. H. and Baldocchi, D. D.: A Biogeochemical Compromise: The High Methane Cost of Sequestering Carbon in Restored Wetlands, Geophys. Res. Lett., 45(12), 6081–6091, doi:10.1029/2018GL077747, 2018.

523 Hines, M. E., Duddleston, K. N., Rooney-Varga, J. N., Fields, D. and Chanton, J. P.:
524 Uncoupling of acetate degradation from methane formation in Alaskan wetlands:
525 Connections to vegetation distribution, Global Biogeochem. Cycles, 22(2), n/a-n/a,
526 doi:10.1029/2006GB002903, 2008.
527 Hinkel, K. M., Frohn, R. C., Nelson, F. E., Eisner, W. R. and Beck, R. A.: Morphometric
528 and spatial analysis of thaw lakes and drained thaw lake basins in the western Arctic
529 Coastal Plain, Alaska, Permafr. Periglac. Process., doi:10.1002/ppp.532, 2005.
530 Hodgkins, S. B., Tfaily, M. M., McCalley, C. K., Logan, T. A., Crill, P. M., Saleska, S. R.,
531 Rich, V. I. and Chanton, J. P.: Changes in peat chemistry associated with permafrost
532 thaw increase greenhouse gas production, Proc. Natl. Acad. Sci.,
533 doi:10.1073/pnas.1314641111, 2014.
534 Iwata, H., Harazono, Y., Ueyama, M., Sakabe, A., Nagano, H., Kosugi, Y., Takahashi, K.
535 and Kim, Y.: Methane exchange in a poorly-drained black spruce forest over
536 permafrost observed using the eddy covariance technique, Agric. For. Meteorol.,
537 214–215, 157–168, doi:10.1016/j.agrformet.2015.08.252, 2015.
538 Kirschke, S., Bousquet, P., Ciais, P., Saunois, M., Canadell, J. G., Dlugokencky, E. J.,
539 Bergamaschi, P., Bergmann, D., Blake, D. R., Bruhwiler, L., Cameron-Smith, P.,
540 Castaldi, S., Chevallier, F., Feng, L., Fraser, A., Heimann, M., Hodson, E. L., Houweling,
541 S., Josse, B., Fraser, P. J., Krummel, P. B., Lamarque, J.-F., Langenfelds, R. L., Le Quéré,
542 C., Naik, V., O'Doherty, S., Palmer, P. I., Pison, I., Plummer, D., Poulter, B., Prinn, R. G.,
543 Rigby, M., Ringeval, B., Santini, M., Schmidt, M., Shindell, D. T., Simpson, I. J., Spahni,
544 R., Steele, L. P., Strode, S. A., Sudo, K., Szopa, S., van der Werf, G. R., Voulgarakis, A.,
545 van Weele, M., Weiss, R. F., Williams, J. E. and Zeng, G.: Three decades of global

546 methane sources and sinks, Nat. Geosci., 6(10), 813–823, doi:10.1038/ngeo1955,
547 2013.
548 Knoblauch, C., Beer, C., Liebner, S., Grigoriev, M. N. and Pfeiffer, E. M.: Methane
549 production as key to the greenhouse gas budget of thawing permafrost, Nat. Clim.
550 Chang., 1–4, doi:10.1038/s41558-018-0095-z, 2018.
551 Malmer, N., Johansson, T., Olsrud, M. and Christensen, T. R.: Vegetation, climatic
552 changes and net carbon sequestration in a North-Scandinavian subarctic mire over
553 30 years, Glob. Chang. Biol., doi:10.1111/j.1365-2486.2005.01042.x, 2005.
554 McCalley, C. K., Woodcroft, B. J., Hodgkins, S. B., Wehr, R. A., Kim, E.-H., Mondav, R.,
555 Crill, P. M., Chanton, J. P., Rich, V. I., Tyson, G. W. and Saleska, S. R.: Methane
556 dynamics regulated by microbial community response to permafrost thaw, Nature,
557 514(7523), 478–481, doi:10.1038/nature13798, 2014.
558 Melton, J. R., Wania, R., Hodson, E. L., Poulter, B., Ringeval, B., Spahni, R., Bohn, T.,
559 Avis, C. A., Beerling, D. J., Chen, G., Eliseev, A. V., Denisov, S. N., Hopcroft, P. O.,
560 Lettenmaier, D. P., Riley, W. J., Singarayer, J. S., Subin, Z. M., Tian, H., Zürcher, S.,
561 Brovkin, V., van Bodegom, P. M., Kleinen, T., Yu, Z. C. and Kaplan, J. O.: Present state
562 of global wetland extent and wetland methane modelling: conclusions from a model
563 inter-comparison project (WETCHIMP), Biogeosciences, 10(2), 753–788,
564 doi:10.5194/bg-10-753-2013, 2013.
565 Myhre, G., D., Shindell, F.-M., Bréon, Collins, W., Fuglestvedt, J., Huang, J., Koch, D.,
566 Lamarque, J.-F., D. Lee, Mendoza, B., Nakajima, T., A. Robock, G. Stephens, Takemura,
567 T. and Zhang, H.: Anthropogenic and Natural Radiative Forcing, in Climate Change
568 2013 - The Physical Science Basis, vol. 23, edited by Intergovernmental Panel on

569 Climate Change, pp. 659–740, Cambridge University Press, Cambridge., 2013.
570 Neubauer, S. C. and Megonigal, J. P.: Moving Beyond Global Warming Potentials to
571 Quantify the Climatic Role of Ecosystems, Ecosystems, 18(6), 1000–1013,
572 doi:10.1007/s10021-015-9879-4, 2015.
573 Olefeldt, D. and Roulet, N. T.: Effects of permafrost and hydrology on the
574 composition and transport of dissolved organic carbon in a subarctic peatland
575 complex, J. Geophys. Res. Biogeosciences, 117(1), 1–15,
576 doi:10.1029/2011JG001819, 2012.
577 Olefeldt, D., Turetsky, M. R., Crill, P. M. and Mcguire, A. D.: Environmental and
578 physical controls on northern terrestrial methane emissions across permafrost
579 zones, Glob. Chang. Biol., 19(2), 589–603, doi:10.1111/gcb.12071, 2013.
580 Perryman, C. R., McCalley, C. K., Malhotra, A., Fahnestock, M. F., Kashi, N. N., Bryce, J.
581 G., Giesler, R. and Varner, R. K.: Thaw Transitions and Redox Conditions Drive
582 Methane Oxidation in a Permafrost Peatland, J. Geophys. Res. Biogeosciences,
583 125(3), doi:10.1029/2019JG005526, 2020.
584 Poulter, B., Bousquet, P., Canadell, J. G., Ciais, P., Peregon, A., Saunois, M., Arora, V. K.,
585 Beerling, D. J., Brovkin, V., Jones, C. D., Joos, F., Gedney, N., Ito, A., Kleinen, T., Koven,
586 C. D., McDonald, K., Melton, J. R., Peng, C., Peng, S., Prigent, C., Schroeder, R., Riley, W.
587 J., Saito, M., Spahni, R., Tian, H., Taylor, L., Viovy, N., Wilton, D., Wiltshire, A., Xu, X.,
588 Zhang, B., Zhang, Z. and Zhu, Q.: Global wetland contribution to 2000–2012
589 atmospheric methane growth rate dynamics, Environ. Res. Lett., 12(9), 094013,
590 doi:10.1088/1748-9326/aa8391, 2017.
591 Rinne, J., Tuittila, E. S., Peltola, O., Li, X., Raivonen, M., Alekseychik, P., Haapanala, S.,

592 Pihlatie, M., Aurela, M., Mammarella, I. and Vesala, T.: Temporal Variation of
593 Ecosystem Scale Methane Emission From a Boreal Fen in Relation to Temperature,
594 Water Table Position, and Carbon Dioxide Fluxes, Global Biogeochem. Cycles, 32(7),
595 1087–1106, doi:10.1029/2017GB005747, 2018.
596 Rydén, B. E. and Kostov, L.: Thawing and Freezing in Tundra Soils, Ecol. Bull., (30),
597 251–281 [online] Available from: http://www.jstor.org/stable/20112776, 1980.
598 Saunois, M., Bousquet, P., Poulter, B., Peregon, A., Ciais, P., Canadell, J. G.,
599 Dlugokencky, E. J., Etiope, G., Bastviken, D., Houweling, S., Janssens-Maenhout, G.,
600 Tubiello, F. N., Castaldi, S., Jackson, R. B., Alexe, M., Arora, V. K., Beerling, D. J.,
601 Bergamaschi, P., Blake, D. R., Brailsford, G., Brovkin, V., Bruhwiler, L., Crevoisier, C.,
602 Crill, P., Covey, K., Curry, C., Frankenberg, C., Gedney, N., Höglund-Isaksson, L.,
603 Ishizawa, M., Ito, A., Joos, F., Kim, H. S., Kleinen, T., Krummel, P., Lamarque, J. F.,
604 Langenfelds, R., Locatelli, R., Machida, T., Maksyutov, S., McDonald, K. C., Marshall, J.,
605 Melton, J. R., Morino, I., Naik, V., O'Doherty, S., Parmentier, F. J. W., Patra, P. K., Peng,
606 C., Peng, S., Peters, G. P., Pison, I., Prigent, C., Prinn, R., Ramonet, M., Riley, W. J., Saito,
607 M., Santini, M., Schroeder, R., Simpson, I. J., Spahni, R., Steele, P., Takizawa, A.,
608 Thornton, B. F., Tian, H., Tohjima, Y., Viovy, N., Voulgarakis, A., Van Weele, M., Van
609 Der Werf, G. R., Weiss, R., Wiedinmyer, C., Wilton, D. J., Wiltshire, A., Worthy, D.,
610 Wunch, D., Xu, X., Yoshida, Y., Zhang, B., Zhang, Z. and Zhu, Q.: The global methane
611 budget 2000-2012, Earth Syst. Sci. Data, 8(2), 697–751, doi:10.5194/essd-8-697-
612 2016, 2016.
613 Saunois, M., Bousquet, P., Poulter, B., Peregon, A., Ciais, P., Canadell, J. G.,
614 Dlugokencky, E. J., Etiope, G., Bastviken, D., Houweling, S., Janssens-Maenhout, G.,

615 Tubiello, F. N., Castaldi, S., Jackson, R. B., Alexe, M., Arora, V. K., Beerling, D. J.,
616 Bergamaschi, P., Blake, D. R., Brailsford, G., Bruhwiler, L., Crevoisier, C., Crill, P.,
617 Covey, K., Frankenberg, C., Gedney, N., Höglund-Isaksson, L., Ishizawa, M., Ito, A.,
618 Joos, F., Kim, H. S., Kleinen, T., Krummel, P., Lamarque, J. F., Langenfelds, R., Locatelli,
619 R., Machida, T., Maksyutov, S., Melton, J. R., Morino, I., Naik, V., O'Doherty, S.,
620 Parmentier, F. J. W., Patra, P. K., Peng, C., Peng, S., Peters, G. P., Pison, I., Prinn, R.,
621 Ramonet, M., Riley, W. J., Saito, M., Santini, M., Schroeder, R., Simpson, I. J., Spahni, R.,
622 Takizawa, A., Thornton, B. F., Tian, H., Tohjima, Y., Viovy, N., Voulgarakis, A., Weiss,
623 R., Wilton, D. J., Wiltshire, A., Worthy, D., Wunch, D., Xu, X., Yoshida, Y., Zhang, B.,
624 Zhang, Z. and Zhu, Q.: Variability and quasi-decadal changes in the methane budget
625 over the period 2000-2012, Atmos. Chem. Phys., 17(18), 11135–11161,
626 doi:10.5194/acp-17-11135-2017, 2017.
627 Schuur, E. A. G., McGuire, A. D., Schädel, C., Grosse, G., Harden, J. W., Hayes, D. J.,
628 Hugelius, G., Koven, C. D., Kuhry, P., Lawrence, D. M., Natali, S. M., Olefeldt, D.,
629 Romanovsky, V. E., Schaefer, K., Turetsky, M. R., Treat, C. C. and Vonk, J. E.: Climate
630 change and the permafrost carbon feedback, Nature, 520(7546), 171–179,
631 doi:10.1038/nature14338, 2015.
632 Shiklomanov, N. I., Streletskiy, D. A., Nelson, F. E., Hollister, R. D., Romanovsky, V. E.,
633 Tweedie, C. E., Bockheim, J. G. and Brown, J.: Decadal variations of active-layer
634 thickness in moisture-controlled landscapes, Barrow, Alaska, J. Geophys. Res.
635 Biogeosciences, doi:10.1029/2009JG001248, 2010.
636 Singleton, C. M., McCalley, C. K., Woodcroft, B. J., Boyd, J. A., Evans, P. N., Hodgkins, S.
637 B., Chanton, J. P., Frolking, S., Crill, P. M., Saleska, S. R., Rich, V. I. and Tyson, G. W.:

638 Methanotrophy across a natural permafrost thaw environment, ISME J., 12(10),
639 2544–2558, doi:10.1038/s41396-018-0065-5, 2018.
640 Tang, J. and Riley, W. J.: Weaker soil carbon-climate feedbacks resulting from
641 microbial and abiotic interactions, Nat. Clim. Chang., advance on(January),
642 doi:10.1038/nclimate2438, 2014.
643 Tøsdal, A., Urich, T., Frenzel, P. and Marianne, M.: Metabolic and trophic interactions
644 modulate methane production by Arctic peat microbiota in response to warming,
645 Proc. Natl. Acad. Sci., E2507–E2516, doi:10.1073/pnas.1420797112, 2015.
646 Updegraff, K., Bridgham, S. D., Pastor, J. and Weishampel, P.: Hysteresis in the
647 temperature response of carbon dioxide and methane production in peat soils,
648 Biogeochemistry, 43(3), 253–272, doi:10.1023/A:1006097808262, 1998.
649 Wainwright, H. M., Dafflon, B., Smith, L. J., Hahn, M. S., Curtis, J. B., Wu, Y., Ulrich, C.,
650 Peterson, J. E., Torn, M. S. and Hubbard, S. S.: Identifying multiscale zonation and
651 assessing the relative importance of polygon geomorphology on carbon fluxes in an
652 Arctic tundra ecosystem, J. Geophys. Res. Biogeosciences,
653 doi:10.1002/2014JG002799, 2015.
654 Wania, R., Melton, J. R., Hodson, E. L., Poulter, B., Ringeval, B., Spahni, R., Bohn, T.,
655 Avis, C. A., Chen, G., Eliseev, A. V., Hopcroft, P. O., Riley, W. J., Subin, Z. M., Tian, H.,
656 Van Bodegom, P. M., Kleinen, T., Yu, Z. C., Singarayer, J. S., Zürcher, S., Lettenmaier, D.
657 P., Beerling, D. J., Denisov, S. N., Prigent, C., Papa, F. and Kaplan, J. O.: Present state of
658 global wetland extent and wetland methane modelling: Methodology of a model
659 inter-comparison project (WETCHIMP), Geosci. Model Dev., 6(3), 617–641,
660 doi:10.5194/gmd-6-617-2013, 2013.

661 Wik, M., Varner, R. K., Anthony, K. W., MacIntyre, S. and Bastviken, D.: Climate-
662 sensitive northern lakes and ponds are critical components of methane release, Nat.
663 Geosci., 9(2), 99–105, doi:10.1038/ngeo2578, 2016.
664 Wohlfahrt, G. and Galvagno, M.: Revisiting the choice of the driving temperature for
665 eddy covariance CO2flux partitioning, Agric. For. Meteorol., 237–238, 135–142,
666 doi:10.1016/j.agrformet.2017.02.012, 2017.
667 Xu, X., Yuan, F., Hanson, P. J., Wullschleger, S. D., Thornton, P. E., Riley, W. J., Song, X.,
668 Graham, D. E., Song, C. and Tian, H.: Reviews and syntheses: Four decades of
669 modeling methane cycling in terrestrial ecosystems, Biogeosciences, 13(12), 3735–
670 3755, doi:10.5194/bg-13-3735-2016, 2016.
671 Yvon-Durocher, G., Allen, A. P., Bastviken, D., Conrad, R., Gudasz, C., St-Pierre, A.,
672 Thanh-Duc, N. and Del Giorgio, P. A.: Methane fluxes show consistent temperature
673 dependence across microbial to ecosystem scales, Nature, 507(7493), 488–491,
674 doi:10.1038/nature13164, 2014.
675 Zhang, L., Liu, X., Duddleston, K. and Hines, M. E.: The Effects of pH, Temperature,
676 and Humic-Like Substances on Anaerobic Carbon Degradation and Methanogenesis
677 in Ombrotrophic and Minerotrophic Alaskan Peatlands, Aquat. Geochemistry,
678 (0123456789), doi:10.1007/s10498-020-09372-0, 2020.
679 Zona, D., Gioli, B., Commane, R., Lindaas, J., Wofsy, S. C. and Miller, C. E.: Cold season
680 emissions dominate the Arctic tundra methane budget, Proc. Natl. Acad. Sci., 113(1),
681 40–45, doi:10.1073/pnas.1516017113, 2016.
682

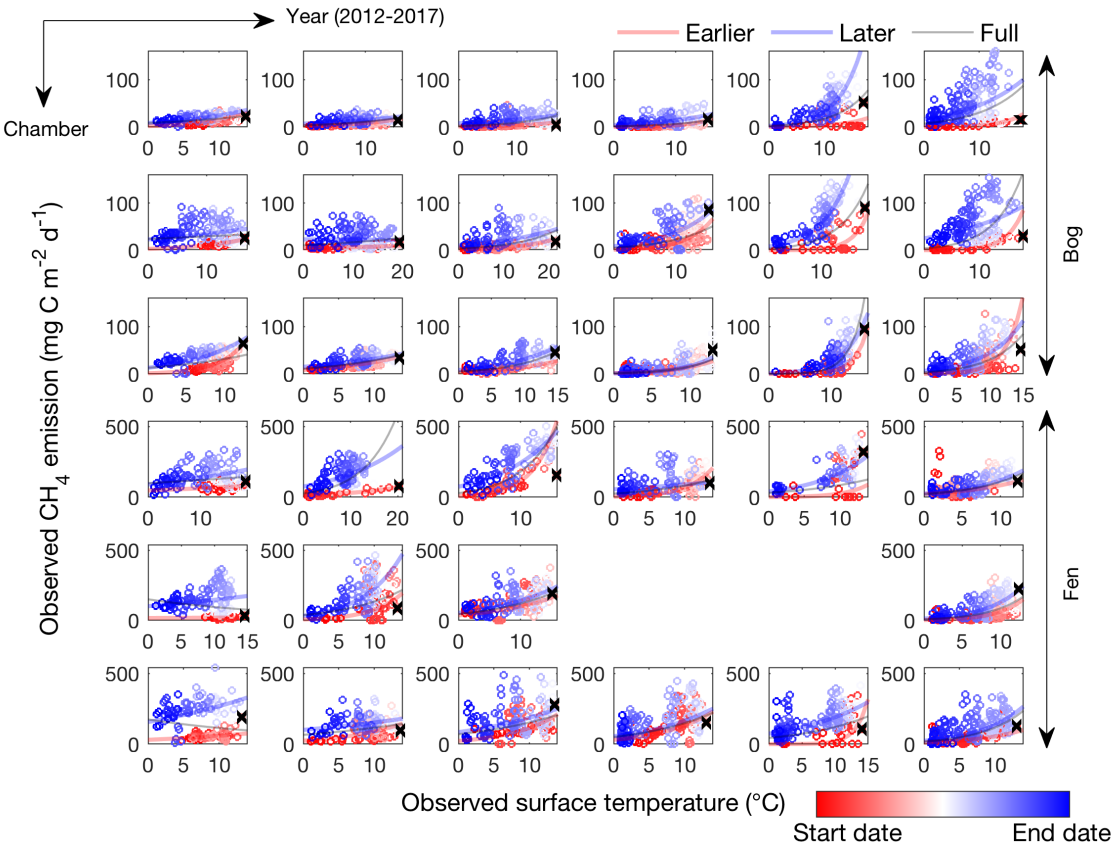

683

684 Figure 1. CH_4 emissions are hysteretic to soil surface temperature measured in individual
685 automated chambers at the Stordalen Mire bog (top three panels) and fen (bottom three
686 panels) sites from 2012 to 2017 thawed seasons (left to right). Open circles and lines
687 represent the daily data points and the fitted apparent CH_4 emission temperature
688 dependence, respectively. The earlier, later, and full-season periods are colored in red,
689 blue, and black, respectively. Earlier and later periods are defined as the time before and
690 after the seasonal maximum soil surface temperature denoted by black cross signs. Start
691 date and end dates represent the beginning and ending of a thawed season defined as the
692 period when measured daily soil surface temperature is above 1 ˚C, respectively.

693

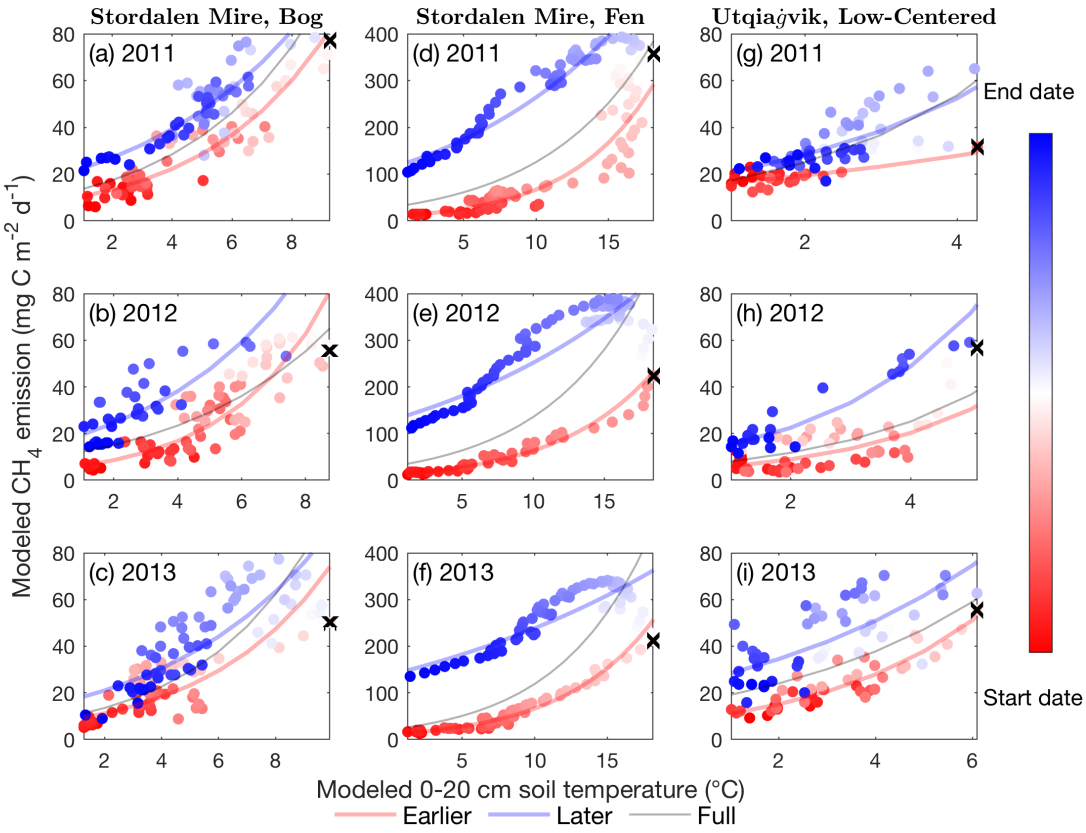

694

695 Figure 2. CH_4 emissions are hysteretic to soil temperature modeled in the Stordalen Mire
696 bog (a to c) and fen (d to f) and the Utqiaġvik low-centered polygon (g to i) from 2011 to
697 2013 thawed seasons. Dots and lines represent the daily data points and the fitted
698 apparent temperature dependence, respectively. Earlier, later, and full-season periods are
699 colored in red, blue, and black, respectively. Earlier and later periods are defined as the
700 time before and after the seasonal maximum 0-20 cm soil temperature denoted by black
701 cross signs. Start date and end dates represent the beginning and ending of a thawed
702 season defined as the period when modeled daily 0-20 cm soil temperature is above 1 ˚C,
703 respectively.

704

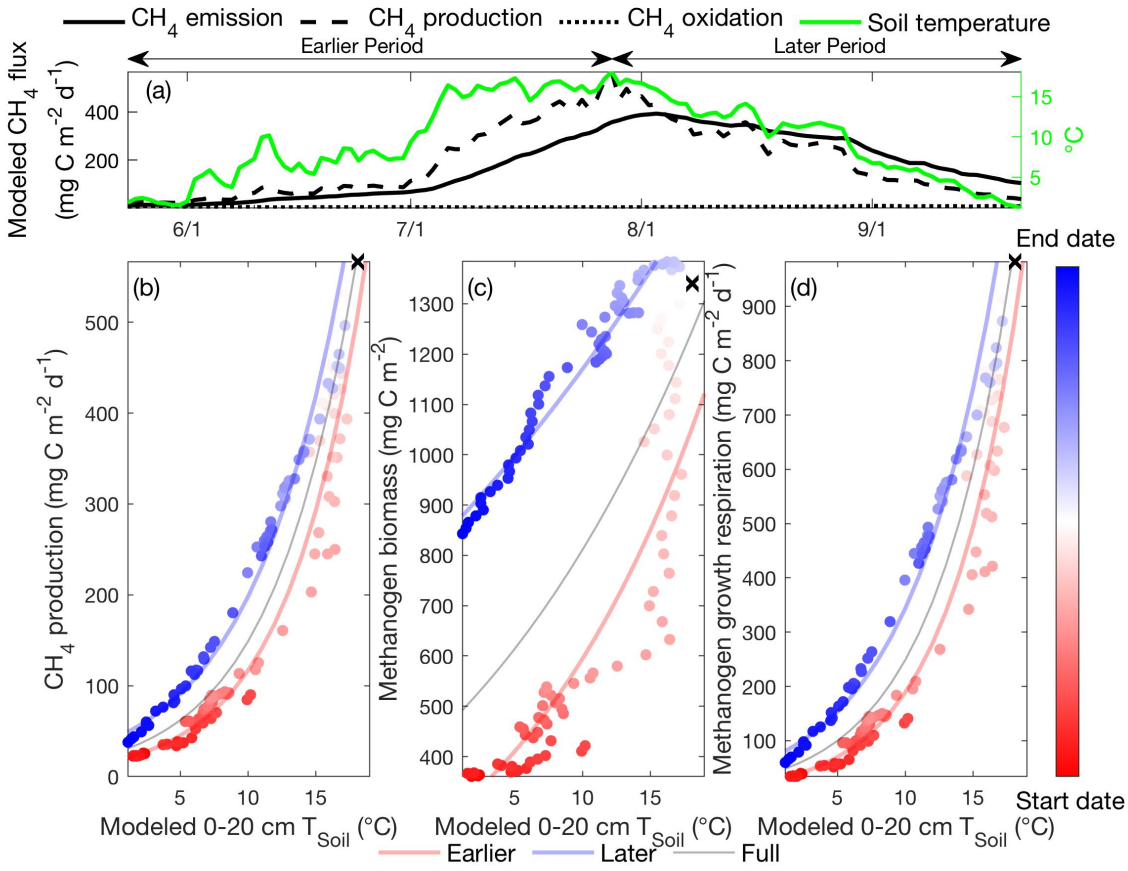

Figure 3. Intra-seasonal variations in apparent CH_4 production temperature dependence result from asymmetric microbial biomass and activity modeled between the earlier and later periods. Daily CH_4 emissions, CH_4 production, CH_4 oxidation, and 0-20 cm soil temperature modeled in the Stordalen Mire fen during the 2011 thawed season (a). The corresponding apparent temperature dependence of the modeled CH_4 production (b), methanogen biomass (c), and methanogen growth respiration (d) during the 2011 thawed season. Earlier, later, and full-season periods are colored in red, blue, and black, respectively. Earlier and later periods are defined as the time before and after the seasonal maximum 0-20 cm soil temperature denoted by black cross signs. Start date and end dates represent the beginning and ending of a thawed season defined as the period when modeled daily 0-20 cm soil temperature is above 1 ˚C, respectively.

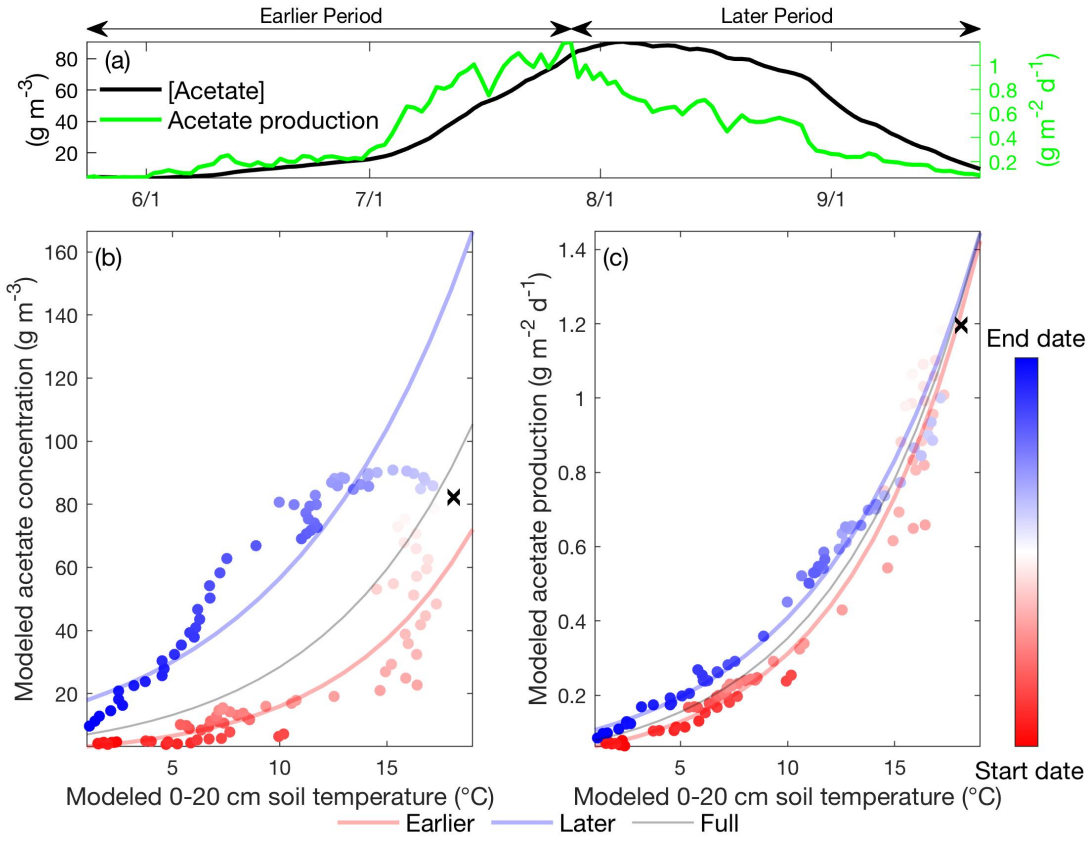

718

719 Figure 4. Daily acetate concentration and acetate production modeled in the Stordalen
720 Mire fen during the 2011 thawed season (a). The corresponding apparent temperature
721 dependence of the modeled acetate concentration (b) and acetate production (c) during
722 the 2011 thawed season. Dots and lines represent the daily data points and the fitted
723 apparent temperature dependence, respectively. The earlier, later, and full-season periods
724 are colored in red, blue, and black, respectively. Earlier and later periods are defined as
725 the time before and after the seasonal maximum 0-20 cm soil temperature denoted by
726 black cross signs. Start date and end dates represent the beginning and ending of a thawed
727 season defined as the period when modeled daily 0-20 cm soil temperature is above 1 ˚C,
728 respectively.

729

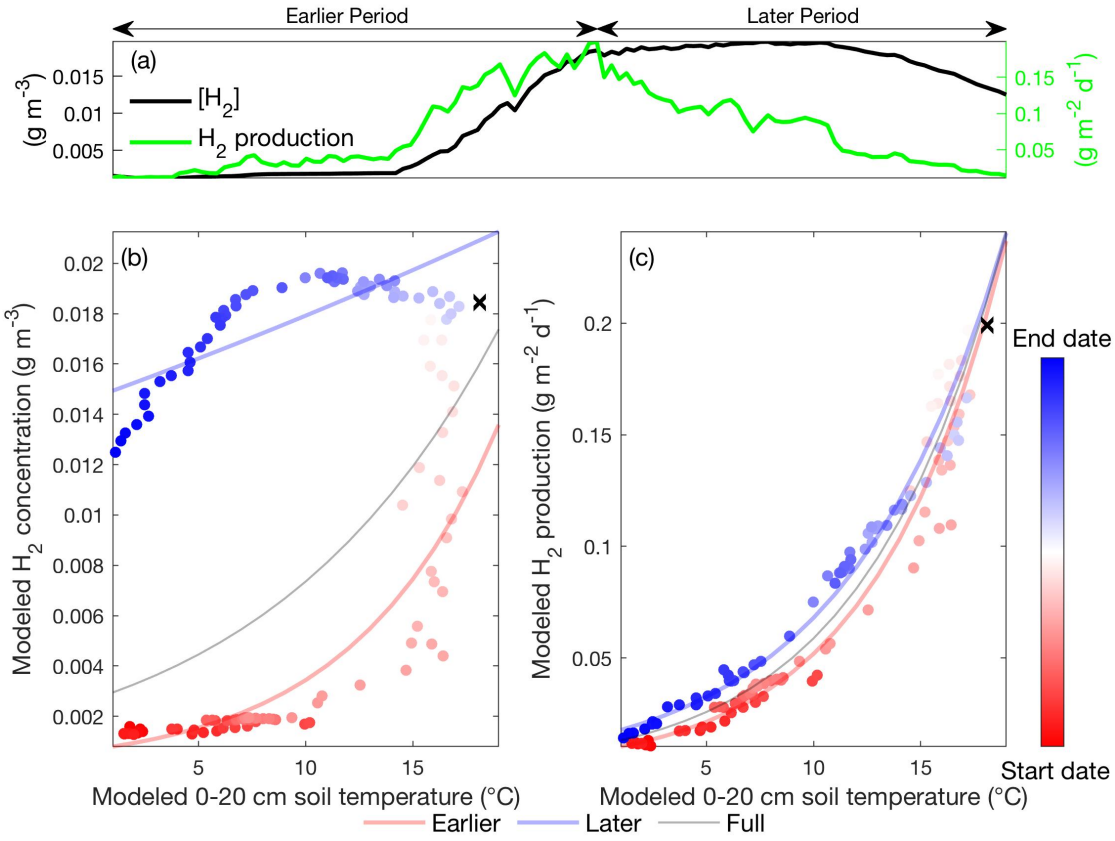

730

731 Figure 5. Daily hydrogen concentration and hydrogen production modeled in the
732 Stordalen Mire fen during the 2011 thawed season (a). The corresponding apparent
733 temperature dependence of the modeled hydrogen concentration (b) and hydrogen
734 production (c) during the 2011 thawed season. Dots and lines represent the daily data
735 points and the fitted apparent temperature dependence, respectively. The earlier, later,
736 and full-season periods are colored in red, blue, and black, respectively. Earlier and later
737 periods are defined as the time before and after the seasonal maximum 0-20 cm soil
738 temperature denoted by black cross signs. Start date and end dates represent the
739 beginning and ending of a thawed season defined as the period when modeled daily 0-20
740 cm soil temperature is above 1 ˚C, respectively.

741

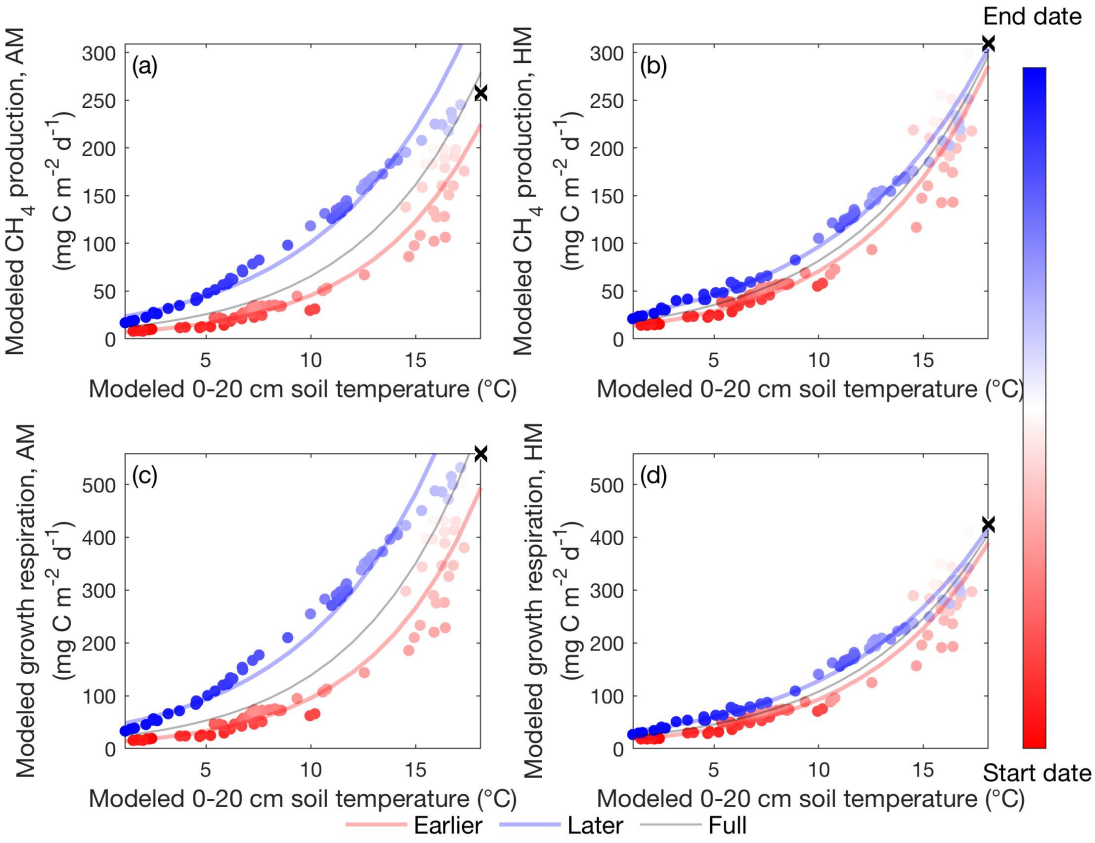

Figure 6. Apparent temperature dependence of daily CH_4 production for acetoclastic (a) and hydrogenotrophic (b) methanogenesis, and daily growth respiration for acetoclastic (c) and hydrogenotrophic (d) methanogens modeled in the Stordalen Mire fen during the 2011 thawed season. Dots and lines represent the daily data points and the fitted apparent temperature dependence, respectively. The earlier, later, and full-season periods are colored in red, blue, and black, respectively. Earlier and later periods are defined as the time before and after the seasonal maximum 0-20 cm soil temperature denoted by black cross signs. Start date and end dates represent the beginning and ending of a thawed season defined as the period when modeled daily 0-20 cm soil temperature is above 1 ˚C, respectively.

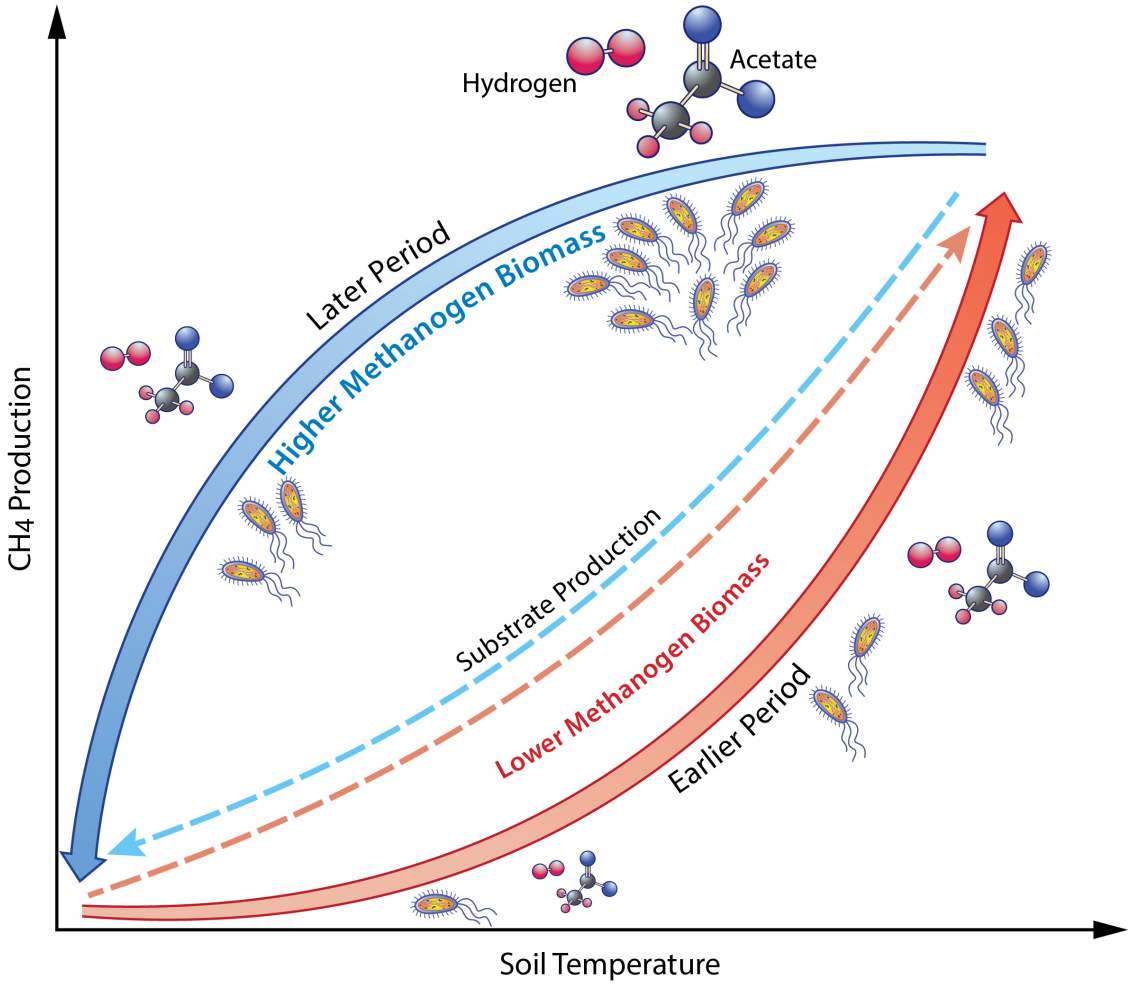

753

754 Figure 7. Schematic of the microbial substrate-mediated CH_4 production hysteresis

755 proposed in this study. Higher substrate (i.e., acetate and hydrogen) availability

756 stimulates higher methanogen biomass during the later period, which leads to intra-

757 seasonal differences in CH_4 production between the earlier and later periods.

758

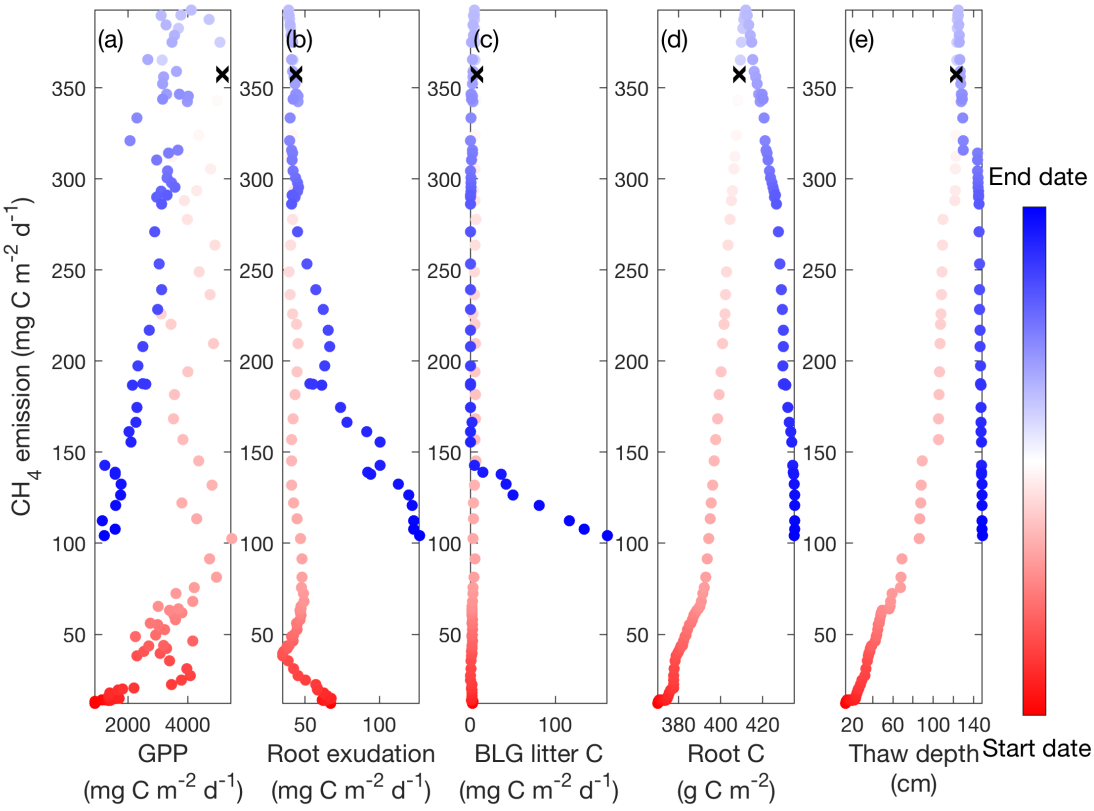

759

760 Figure 8. Daily CH_4 emissions have hysteretic responses to gross primary productivity
761 (a), carbon released from root exudation (b), carbon released from belowground litter
762 decomposition (c), the amount of root biomass for sedges (d), and thaw depth (e)
763 modeled in the Stordalen Mire fen during the 2011 thawed season. Dots and lines
764 represent the daily data points and the fitted apparent temperature dependence,
765 respectively. Black cross signs represent the seasonal maximum 0-20 cm soil
766 temperature. Start date and end dates represent the beginning and ending of a thawed
767 season defined as the period when modeled daily 0-20 cm soil temperature is above 1 ˚C,
768 respectively.

769

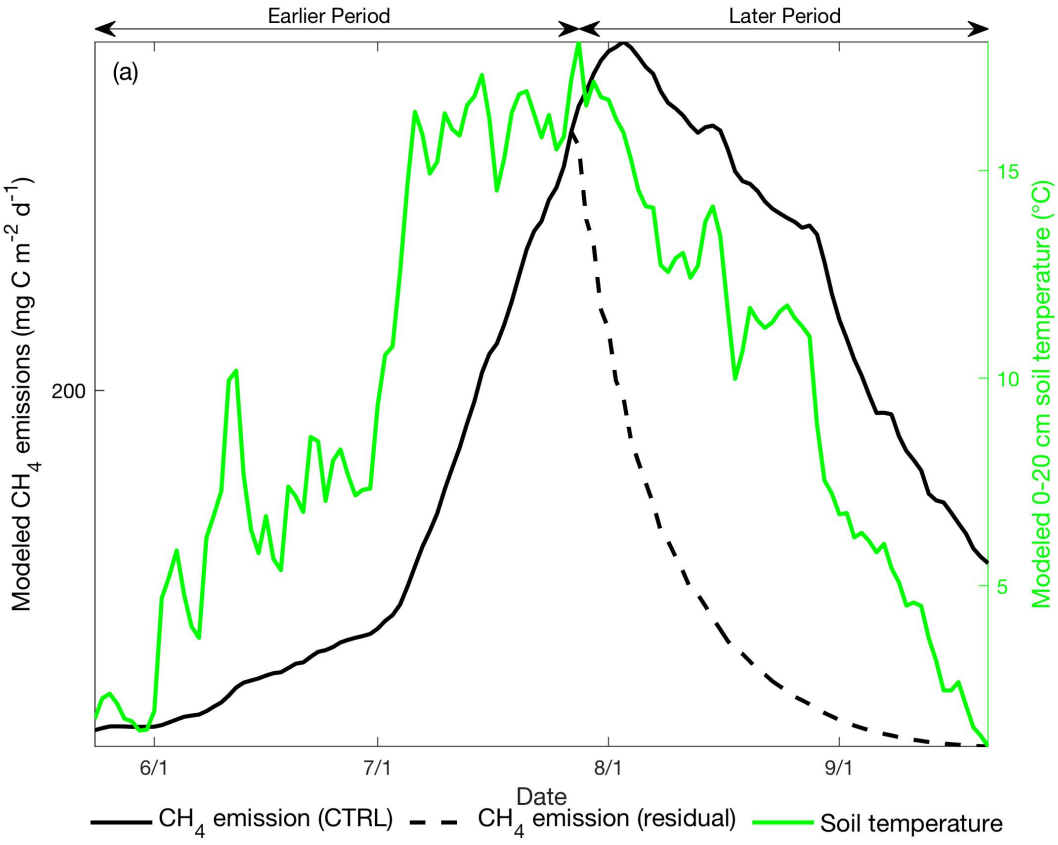

770

771 Figure 9. Daily CH_4 emissions (black line, left axis) and 0-20 cm mean soil temperature

772 (green line, right axis) modeled at the Stordalen Mire fen during the 2011 thawed season.

773 Black solid and dashed lines represent the modeled CH_4 emissions with and without CH_4

774 production during the later period, respectively. Earlier and later periods are defined as

775 the time before and after the modeled seasonal maximum 0-20 cm soil temperature.

776

777